ACS APPLIED MATERIALS & INTERFACES

Research Article

www.acsami.org

Magnetic Field Switchable Dry Adhesives

Jeffrey Krahn, Enrico Bovero, and Carlo Menon*

MENRVA Research Group, School of Engineering Science, Simon Fraser University, Burnaby, British Columbia V5A 1S6, Canada

ABSTRACT: A magnetic field controllable dry adhesive device is manufactured. The normal adhesion force can be increased or decreased depending on the presence of an applied magnetic field. If the magnetic field is present during the entire normal adhesion test cycle which includes both applying a preloading force and measuring the pulloff pressure, a decrease in adhesion is observed when compared to when there is no applied magnetic field. Similarly, if the magnetic field is present only during the preload portion of the normal adhesion test cycle, a decrease in adhesion is observed because of an increased stiffness of the magnetically controlled dry adhesive device. When the applied magnetic field is present during only the pulloff portion of the normal adhesion test cycle, either an increase or a decrease in normal adhesion is observed depending on the direction of the applied magnetic field.

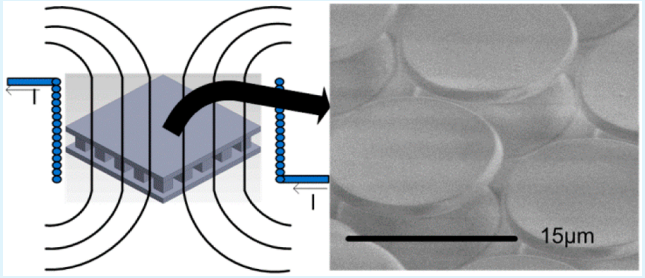

KEYWORDS: *mushroom caps, dry adhesive, magnetic, force, polymer, biomimetic*

1. INTRODUCTION

Since 2000, when evidence that van der Waals' interactions were the main contributors to gecko adhesion force was discovered,[1,2] a great number of research groups have spent considerable effort in fabricating synthetic gecko adhesives. The ability of geckos to adhere to a wide variety of surfaces has inspired researchers to develop synthetic gecko tape which also relies mainly on van der Waals' forces for adhesion. The first attempts at producing synthetic gecko tape were performed by nanoindenting followed by the molding of poly-(dimethylsiloxane) (PDMS) in nanoindented cavities.[3] Other fabrication techniques for producing biomimetic dry adhesive fibers soon followed and include electron beam lithography,[4] plasma etching,[5] photolithography,[6,7] and molding PDMS using commercially available mesh.[8] While some groups have concentrated their efforts on developing new fabrication techniques that allow increased fiber density,[9] other researchers have examined the effect of fiber tip shape,[10,11] fiber aspect ratio, and the addition of an overhanging cap.[12−15] Still others have tried to mimic the structures found on geckos by developing hierarchical structures,[16,17] which increase the ability of the gecko fibers to conform to a surface.

Other approaches to increasing adhesion have been presented such as the synergistic combination of electrostatics and gecko tape where embedded particles[24,25] or chemically etched mesh[26] was used as electrodes to generate electrostatic forces. Still other researchers have embedded magnets onto the ends of large macroscale polymer fibers[27] or have dispersed carbonyl iron particles in a PDMS network to form magnetically actuated gecko microridges[28] or beams.[29]

In the meantime, another approach to increasing adhesion has been to change the stiffness of the backing layer to resist peeling as described in our earlier work[18] where a phase-change material was used to conform to the surface of a spherical probe when in the softer phase but to resist peeling when in a hardened phase. Switchable adhesion has also been achieved with thermally controlled shape memory polymers being used as either a backing layer[19] or for bending the fibers themselves.[20] Switchable adhesion has also been shown through the use of microchannels[21] within a backing layer, contact surface area decrease through a thin film surface collapse[22] or by surface wrinkling.[23]

Recently, several research groups have studied the effect of magnetorheological elastomers (MRE) made from PDMS and carbonyl iron particles. In the presence of a magnetic field, the MRE show an increase in shear modulus as the intensity of the magnetic field increases,[30,31] and a theoretical model explaining the change in the modulus of MRE because of the presence of a magnetic field has been developed.[32,33] Other recent work on magnetically controlled elastomers includes a magnetic micro-fluidic mixer where the magnetic elastomer was used as a magnetically controllable valve.[34]

In this study, a magnetically controlled dry adhesive device is fabricated by dispersing iron oxide particles in a PDMS matrix. In the presence of an applied magnetic field, the stiffness of the devices' backing layer increases as has been shown previously by others.[32,35,36] The increase in the stiffness of the backing results in increased adhesion because a stiffer backing layer resists peeling. Unlike the magnetic actuated dry adhesives described by Gillies et al.,[28] which show decreased adhesion when the fibers are bent away from the contact surface and which are designed for adhering to particles, this work describes adhesion switching due to an increase in the stiffness of the backing layer in the presence of a magnetic field. Our device is

Received: August 5, 2014
Accepted: January 15, 2015
Published: January 15, 2015

DOI: 10.1021/am505140f
ACS Appl. Mater. Interfaces 2015, 7, 2214−2222

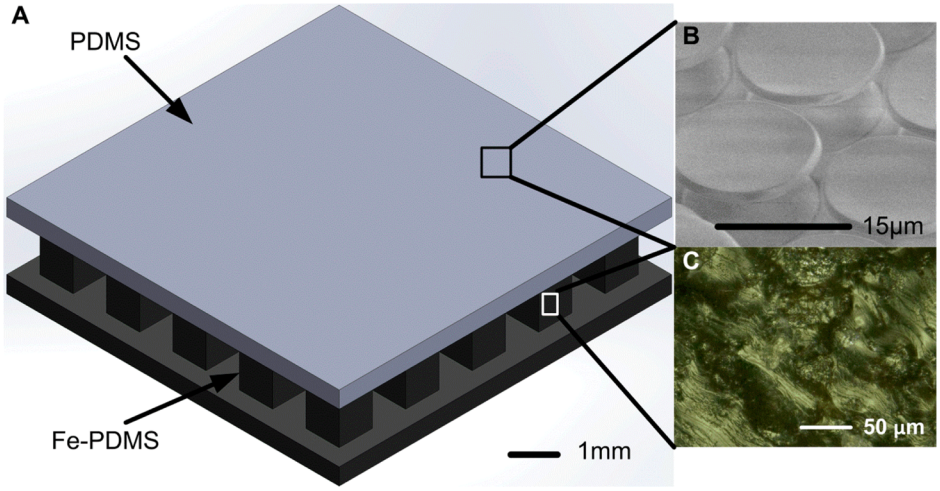

Figure 1. (A) An illustration of the fabricated device showing the PDMS and Fe-PDMS layers. (B) A scanning electron microscope image of the microscale features fabricated from PDMS. (C) Typical cross section of the Fe-PDMS layer showing agglomerations of the 20−30 nm iron oxide nanoparticles within the PDMS.

designed for potentially adhering to large surface areas as opposed to individual particles. The adhesion provided by our device is dependent on which portion of the normal adhesion test cycle the magnetic field is applied and on the direction of the magnetic field; either an increase or decrease in adhesion is observed over the measured normal adhesion force as compared to when no applied magnetic field is present.

2. METHODS AND MATERIALS

2.1. Configuration. The magnetically controlled dry adhesive devices used in this study were fabricated from a polymer matrix of PDMS and 20−30 nm iron oxide nanoparticles (Fe_3O_4, 3320DX SkySpring Nanomaterials Inc.) herein referred to as Fe-PDMS. The overall structure was composed of a thin layer of mushroom-like dry adhesive fibers fabricated from PDMS. The backing layer was constructed of 1.2 mm × 1.2 mm macroscale Fe-PDMS posts, which were each 1.5 mm tall sandwiched between two thin flat layers of Fe-PDMS. The PDMS microstructured layer was bonded directly to the Fe-PDMS by a thin layer of Fe-PDMS.

2.2. Fabrication. To fabricate the magnetically switchable adhesive devices, several fabrication stages were required. First, a mold in which to cast the microscale features had to be fabricated in a process that was similar to those reported previously.[18,24,39] The fabrication of the mold used to define the microscale feature began with spin-coating a 100 mm diameter poly(methyl methacrylate) (PMMA) wafer with a thin layer of PMGI SF19 resist. After performing a 2 min soft bake at 100 °C, a layer of AZ 9260 photoresist was spin-coated over the PMGI layer. The PMMA wafer with the two resist layers was then placed in a thermal chamber and was baked for 1 h at 80 °C followed by 90 s at 100 °C. After allowing the wafer to cool, the wafer was soaked in a deionized (DI) water bath for 30 min. After the rehydration step was completed, the photoresist layers were exposed to i-line UV light to transfer the mask pattern to the resist before the resist layers were developed in AZ 400 K diluted in a 1:4 ratio by volume with DI water. After achieving the desired undercut, which corresponds to the overhanging mushroom cap of the dry adhesive fibers, a mold with an array of microscale holes which define the shape of the mushroom-like dry adhesive fibers was complete.

Once a suitable mold had been fabricated, PDMS (Sylgard 184) was mixed in a 10:1 ratio of prepolymer to curing agent and was degassed within a vacuum chamber before being spin-coated onto the wafer mold. In the meantime, another mold had been fabricated from PMMA using a laser cutter which cut an array of macroscale 1.2 mm × 1.2 mm square holes into the 1.5 mm thick PMMA. After bonding the PMMA with the array of macroscale holes to another flat piece of PMMA, a mold capable of forming 1.2 mm × 1.2 mm × 1.5 mm tall square posts was achieved. After mixing another batch of PDMS, again in a ratio of 10:1 prepolymer to curing agent by weight, 20−30 nm diameter iron oxide particles (Fe_3O_4, 3320DX SkySpring Nanomaterials Inc.) were introduced and were thoroughly mixed into the PDMS. The iron oxide particles made up 50% of the total weight of the Fe-PDMS. The choice to fabricate the switchable dry adhesion device using a 50% concentration of iron oxide particles was due to two factors: an increased concentration of particles resulted in an increased adhesion switching effect, but iron oxide concentrations greater than 50% were difficult to reliably degas and to remove unwanted air pockets during fabrication. After carefully spreading the Fe-PDMS over both the macroscale featured mold and the cured PDMS on the microscale featured mold, the Fe-PDMS was degassed in a vacuum chamber for a period of several hours before finally curing the Fe-PDMS in a thermal chamber at 80 °C for several hours. After demolding the cured Fe-PDMS from the macroscale featured mold, the tips of the 1.2 mm × 1.2 mm posts were bonded to the Fe-PDMS on the unstructured side of the microscale featured mold using a small amount of Fe-PDMS. After demolding from the microscale featured mold, the magnetically controlled dry adhesive device was ready for use. A diagram of the completed device is shown in Figure 1.

2.3. Testing. The test setup, as illustrated in Figure 2, was composed of the magnetic switchable dry adhesive device placed at the center of a wire coil. Testing was performed with either a 6 mm or a 12 mm diameter spherical glass probe tip mounted to a load cell (Futek, LRF 400) with a Nylon screw that was sufficiently long enough to ensure that any magnetic field applied to the sample did not noticeably affect the load cell reading, and any effect of switching the magnetic field on or off on the load cell is below the sensitivity of the load cell. This was confirmed by placing the probe tip at multiple locations both near and away from the surface of the sample under test and switching the magnetic field on and off repeatedly with the magnetic field orientated in both directions. The load cell was mounted on a linear stage (Zaber, T-LS28M-S) which controlled the traveling speed and direction of the probe. The applied magnetic field was produced by a wire coil (APW Company, FC-6489) and was measured using a Hall effect sensor (OHS3150U, OPTEK Technology Inc.).

3. RESULTS AND DISCUSSION

The overall structure of the device was designed to take advantage of the embedded iron oxide particles which, in the presence of a sufficiently strong magnetic field, caused the overall stiffness of the Fe-PDMS material forming the backing layer to increase, while maintaining the strong adhesive

DOI: 10.1021/am505140f
ACS Appl. Mater. Interfaces 2015, 7, 2214−2222

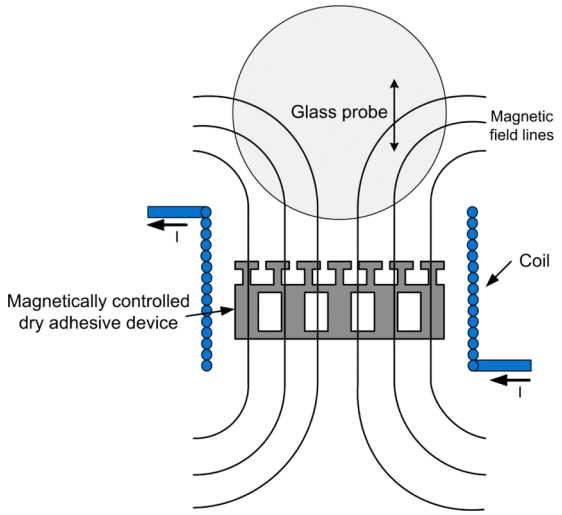

Figure 2. A diagram of the test setup. The magnetically controlled dry adhesive device was placed at the center of a wire coil, and normal adhesion force tests were performed without a current applied to the coil and with a current applied to the coil in both directions resulting in two different magnetic field orientations.

capabilities of PDMS-based dry adhesives. To provide a comparison of the adhesion change the magnetic switchable dry adhesive device was capable of providing, a series of tests were performed.

First, however, to characterize the magnetic field generated by the coil, a Hall effect sensor (OHS3150U, OPTEK Technology Inc.) was used. The magnetic field profile was measured both from the upper to lower edges of the coil along the central axis of the coil and across the diameter of the coil at approximately the midway point between the top and the bottom surfaces of the coil. The maximum field strength, as shown in Figure 3, was measured to be 0.0126 ± 0.0009 T at

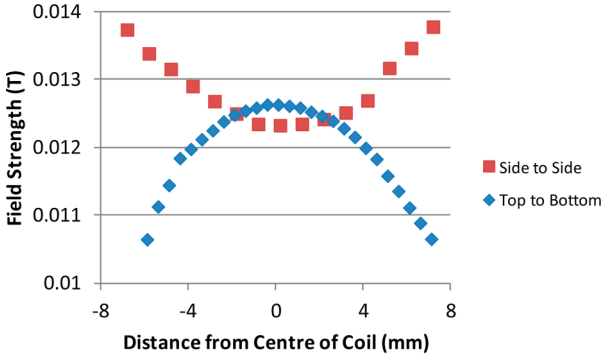

Figure 3. Measured change in magnetic field strength from the top surface of the coil to the bottom surface along the central axis of the coil and across the diameter of the coil at the midway point between the upper and lower surfaces of the coil. The measured magnetic field strength was measured to be 0.0133 ± 0.0009 T at the surface of the device during testing.

the center of the coil at a distance of 6.21 ± 0.01 mm from the upper edge of the coil. As can be seen in Figure 3, at the midway point between the upper and lower surfaces of the coil, the magnetic field varied across the diameter of the coil from a maximum of 0.0146 ± 0.0009 T near the edge of the coil to a minimum of 0.0123 ± 0.0009 T at the center of the coil. The measurements of the magnetic field strength were performed with the magnetic field in orientation 1 which corresponds to the current moving through the coil in the counterclockwise direction.

As described previously, during the fabrication process, iron oxide particles were mixed into PDMS to form the Fe-PDMS magnetically controlled dry adhesive device. Each iron oxide particle acted as a magnetic dipole and, when mixed together and cured in the PDMS, the magnetic dipole of each particle contributed to the net magnetic field of the magnetically controlled dry adhesive device. The net magnetic field of the magnetically controlled dry adhesive device is related to the fabrication process and is due to the mixing process where the particles are oriented in a random fashion and are free to agglomerate before and during curing. As the Fe-PDMS is curing, the particles are free to rotate within the Fe-PDMS, and the net effect is that they are able to align themselves with each other and with any external magnetic field. The net magnetic field of the magnetically controlled dry adhesive device could be measured using a Hall effect sensor and was determined to be 0.00023 ± 0.00009 T at the surface of the microscale structures. The south pole of the device was determined to be facing away from the device on the upper surface at an angle, θ, of 38° as shown in Figure 4 A. When the magnetically controlled dry adhesive device was placed in an applied magnetic field, the magnetically controlled dry adhesive device would increase its stiffness and its height would change as the particles embedded within the PDMS matrix would try and align themselves with the magnetic field as illustrated in Figure 4. The dry adhesive fibers on the surface of the magnetically controlled dry adhesive device were 12 μm tall with a 15 μm diameter cap and 1.8 μm thick overhanging cap atop a 12.5 μm diameter post. The center-to-center spacing of the fibers was 20 μm, and the adhesive fibers created by the mold are shown in Figure 1B. The PDMS layer which defined the microscale features was 75 μm thick.

To determine the effective Young's modulus of the magnetically controlled dry adhesive device, the applied compressive load along with the indentation depth of the spherical indenter was measured. Hertz theory of elastic contact between a spherical indenter and a flat surface, ignoring the effect of the microscale features, was used to estimate the effective Young's modulus $E^* = E/(1 - \nu^2)$, where $\nu \approx 0.5$ is Poisson's ratio. The Young's modulus of PDMS is approximately 2 MPa. The effective Young's modulus was determined by fitting the experimental data to

$$F = \frac{4}{3}E^*\sqrt{Rd^3} \quad (1)$$

where F is the applied preload, R is the radius of the indenting sphere, and d is the indentation depth.[40] The indentation depth of the glass sphere was directly determined by subtracting the linear stage position when contact with the surface of the device was initiated from the position of the stage at the desired preload depth and was confirmed to be an accurate determination of the indentation depth of the sphere on the basis of images taken with a digital microscope (Keyence, VHX-2000) fitted with a 100−1000X wide range zoom lens (Keyence, VH-Z100WS).

Figure 5 A and B shows the indentation depth-preload and preload-distance curves, respectively, for the magnetically controlled dry adhesive device without the magnetic field applied and with the 0.0133 ± 0.0009 T magnetic field applied in both orientation 1 (current flowing counterclockwise) and

DOI: 10.1021/am505140f
ACS Appl. Mater. Interfaces 2015, 7, 2214−2222

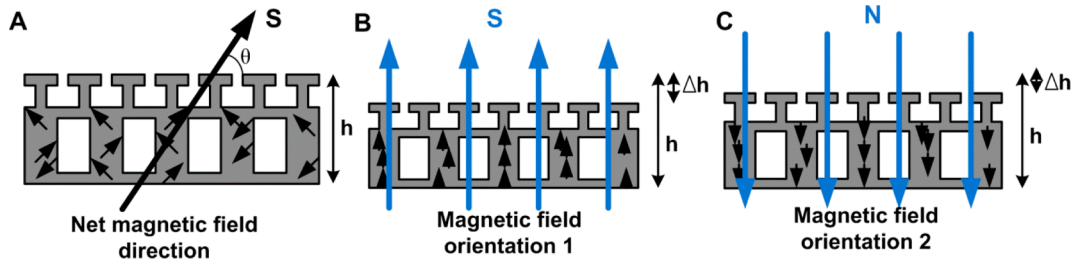

Figure 4. (A) An illustration of the net magnetic field generated by the iron oxide particles within the Fe-PDMS. Placing the magnetically controlled dry adhesive device in the presence of a sufficiently strong magnetic field in (B) orientation 1 and (C) orientation 2 results in an increase in the stiffness of the Fe-PDMS material.

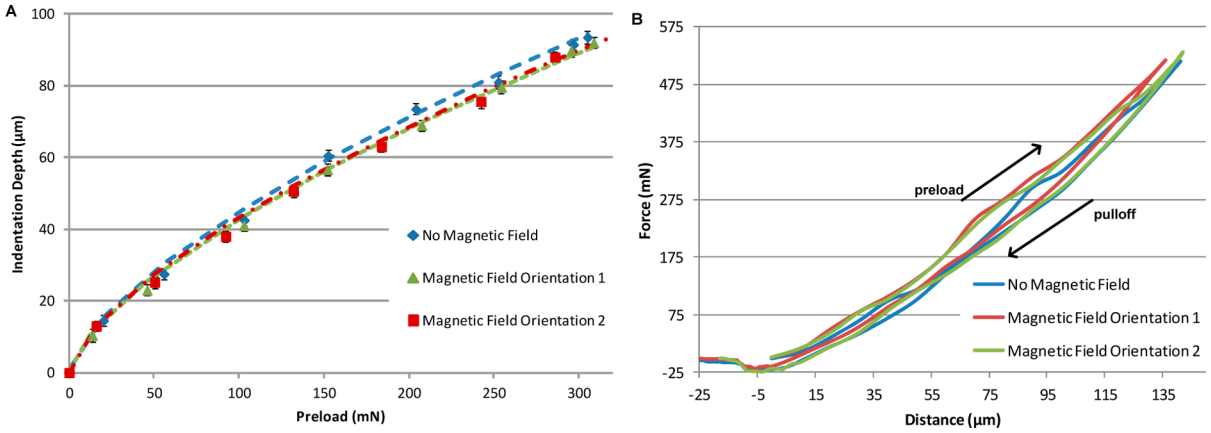

Figure 5. (A) Preload-compression curves. (B) Typical force−distance curves for a 6 mm diameter spherical probe indenting the surface of the magnetically controlled adhesive device with no applied magnetic field present and the 0.0133 ± 0.0009 T magnetic field present during preload and pulloff in either orientation 1 or orientation 2. In A, the dashed lines were fit to the experimental data using eq 1 and were used to estimate the effective Young's modulus. Each data point represents the average indentation depth over a period of three trials, and the error bars represent the standard deviation.

orientation 2 (current flowing clockwise). The sample was loaded at a constant rate of 5 μm/s, and testing was performed on the same location for each set of tests. Each data point in Figure 5 A reflects the average of three separate tests, and the error bars indicate the standard deviation. To minimize any residual effect of the presence of the magnetic field on the device on the test results, there was a minimum waiting period of 10 min between each test, and testing was performed in the following order: one test with no applied magnetic field, one test with the magnetic field applied in orientation 1 followed by one test with the magnetic field applied in orientation 2 before performing the second and third set of tests in the same order. After fitting eq 1 to the data shown in Figure 5, the effective Young's modulus was estimated to be 4.41 ± 0.06 MPa with no magnetic field present and 4.92 ± 0.21 MPa or 4.82 ± 0.16 MPa with the magnetic field present in orientations 1 or 2, respectively. The increase in the effective Young's modulus indicates that the magnetically controlled dry adhesive device becomes stiffer in the presence of an applied magnetic field. Because of the design of the device with a 75 μm thick layer of PDMS defining the surface features, the difference in indentation depths under preloading, as seen in Figure 5, becomes apparent for preloads greater than ∼100 mN. On the basis of the measured magnetic field strength of the coil shown in Figure 3, it is unlikely that there is a significant variation in magnetic field strength for the indentation depths at which testing took place. While we were unable to accurately measure the switching speed of the magnetically controlled dry adhesive device, in our experience, the effect of switching the magnetic field on or off is immediately noticeable.

To compare the effect of the application of a magnetic field on the adhesion provided by the magnetically controlled dry adhesive device, several different series of tests were performed with 20 normal adhesion trials performed for each test. The average preloading force was the same for all trials and was 311.2 ± 7.4 mN. The preloading force was chosen on the basis of maximizing the magnetic field switching effect of our magnetically controlled dry adhesive device while maximizing the adhesion force as tests performed at higher preloads without the magnetic field present did not show a significant increase in adhesion. For each test, the preloading force was achieved using a force feedback loop in our custom LabView software which varied the loading rate from 100 μm/s decreasing to as low as 1 μm/s as the measured preload approached the desired preload. Pulloff measurements were all performed with the stage moving at a rate of 200 μm/s. Furthermore, the sample was allowed to relax for a minimum of 10 min between trials to minimize any residual effects of the presence of the applied magnetic field on the magnetically controlled dry adhesive device, and the trials took place over a period of a few days. Multiple sets of trials indicate that the order of testing did not significantly affect the normal adhesion.

For the first set of trials, the normal adhesion pressure was measured using the test setup previously described in Figure 2 but without any current flowing through the coil and thus without an applied magnetic field present. The average maximum normal adhesion pressure was measured to be

DOI: 10.1021/am505140f
ACS Appl. Mater. Interfaces 2015, 7, 2214−2222

101.4 ± 4.2 kPa, as shown in Figure 6, with an apparent contact area of 1.00 ± 0.03 mm^2. The apparent contact area of the

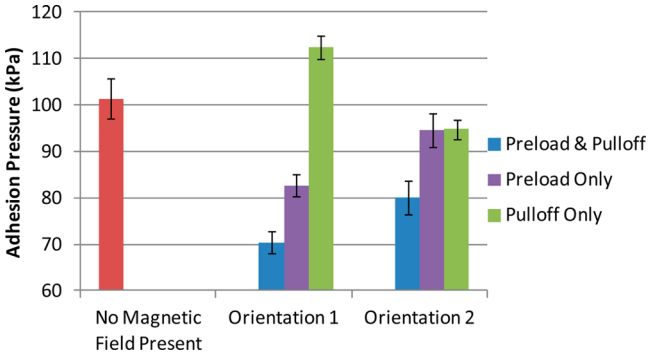

Figure 6. A comparison between the normal adhesion force when there was no magnetic field present and when the magnetic field was present in orientation 1 or orientation 2 during both preloading and pulloff, during preload only, and during pulloff only. Error bars indicate the standard deviation for each set of measurements, and each data point represents the average adhesion pressure over a period of 20 trials.

sphere, A, was calculated on the basis of the measured indentation depth, d, of the glass spherical probe with radius R using

$$A = \pi R d \tag{2}$$

The second set of tests compared the measured normal adhesion force when the 0.0133 ± 0.0009 T magnetic field was present in either orientation 1 or orientation 2 during the entire normal adhesion test cycle which includes during both preloading and pulloff force measurements. As can be seen in Figure 6, under an average applied preloading force of 311.2 ± 7.4 mN, the average normal adhesion pressure decreased to 70.4 ± 2.5 kPa with the magnetic field present in orientation 1 and to an average normal adhesion pressure of 80.1 ± 6.9 kPa with the magnetic field applied in orientation 2. The apparent contact areas were determined by measuring the indentation depth of the spherical probe and were found to be 1.00 ± 0.03 mm^2 and 0.95 ± 0.02 mm^2, respectively.

The decrease in adhesion observed in the presence of the magnetic field when it was applied in either direction during both preload and pulloff portions of the adhesion test cycle is due to the increase in stiffness of the magnetically controlled dry adhesive device in the presence of the magnetic field as indicated in Figure 5. The increased stiffness of the magnetically controlled dry adhesive device results in a smaller contact area for the spherical probe when undergoing the same average 311.2 ± 7.4 mN preload in the presence of the magnetic field as compared to without the applied magnetic field present. The decrease in contact area to achieve the same preload during preloading results in a subsequent decrease in normal adhesion force in the presence of the magnetic field. The difference in adhesion pressure seen between the two magnetic field orientations is likely due to the difference in the stiffness of the device in the presence of the magnetic field in different orientations as the effective Young's modulus is highest when the magnetic field was applied in orientation 1.

The third set of normal adhesion tests was performed with the 0.0133 ± 0.0009 T magnetic field present in either orientation 1 or orientation 2 during only the preloading portion of the normal adhesion test cycle. As can be seen in Figure 6, a decrease in adhesion was observed with the magnetic field present in either direction. With the 0.0133 ± 0.0009 T magnetic field present in orientation 1 during only the preloading portion of the normal adhesion test cycle, the average normal adhesion pressure was measured to be 82.7 ± 2.3 kPa, and with the magnetic field present in orientation 2, the average normal adhesion pressure was measured to be 94.6 ± 3.4 kPa. The apparent area in contact in each case was determined to be 0.97 ± 0.03 mm^2 and 0.99 ± 0.03 mm^2, respectively. As mentioned before, the average preload for all normal adhesion trials was 311.2 ± 7.4 mN. Again, the decrease in normal adhesion force is due to the increased stiffness of the magnetically controlled dry adhesive device in the presence of an applied magnetic field during the preloading portion of the normal adhesion force testing cycle which results in a lower contact area as compared to when no magnetic field is present. A slight increase in normal adhesion force is observed as compared to when the magnetic field is present during both preload and pulloff, which is due to the decrease in the stiffness of the magnetically controlled dry adhesive device during the pulloff portion of the normal adhesion test cycle. After the desired preload is achieved, the applied magnetic field is switched off, and the magnetically controlled dry adhesive device relaxes into its softer phase resulting in a slight increase in contact area which results in an increased adhesion force and adhesion pressure.

The final set of normal adhesion tests involved performing normal adhesion pressure measurements with the applied 0.0133 ± 0.0009 T magnetic field present during only the pulloff portion of the normal adhesion test cycle. As shown in Figure 6, over a period of 20 trials for each test, the average normal adhesion pressure was measured to be 112.5 ± 2.6 kPa with the magnetic field present in orientation 1. With the 0.0133 ± 0.0009 T magnetic field present in orientation 2, however, a decrease in the average normal adhesion pressure was observed as compared to when no applied magnetic field was present. The average measured normal adhesion pressure with the magnetic field present in orientation 2 was 94.8 ± 2.1 kPa. The average apparent area in contact was 1.00 ± 0.03 mm^2 with no applied magnetic field present, 0.99 ± 0.02 mm^2 with the magnetic field applied in orientation 1, and 1.02 ± 0.02 mm^2 with the magnetic field applied in orientation 2. An analysis of variance (ANOVA) was performed to determine if the adhesion results when there was no magnetic field were statistically significant from when the magnetic field was applied in either orientation 1 or 2 during pulloff. The F-value was 182.17 while the $F_{critical}$-value was 3.179 indicating that the results were in fact statistically significant.

To ensure that the changes in adhesion observed when the magnetic field was applied during pulloff were not due to the measured contact area being roughly the same size as the macroscale posts forming the backing layer, testing was also performed with a 12.93 mm diameter glass spherical tip. Figure 7 compares the adhesion pressure between when there was no applied magnetic field present and when the magnetic field was applied in orientations 1 and 2 during pulloff only. The average preloading force for all three sets of tests was 1.013 ± 0.005 N, and the average contact area for all tests was 4.83 ± 0.03 mm^2. Each data point shows the average adhesion pressure for 10 tests, and the error bars represent the standard deviation.

To determine if the increase in adhesion was caused by the change in stiffness of the magnetically controlled dry adhesive device or by another process such as an increase or decrease in

DOI: 10.1021/am505140f
ACS Appl. Mater. Interfaces 2015, 7, 2214−2222

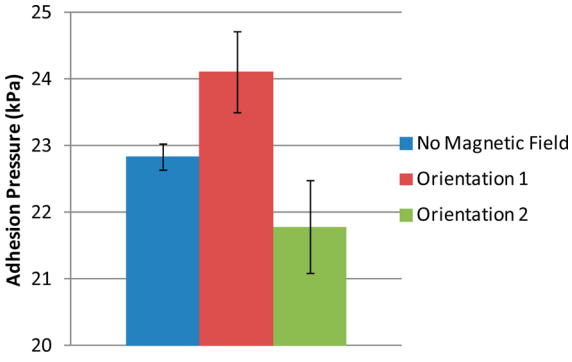

Figure 7. A comparison of the average measured adhesion pressure using a 12.93 mm diameter spherical glass probe when there was no applied magnetic field present and when the magnetic field was applied during pulloff in both orientations 1 and 2. Errors bars represent the standard deviation, and each data point represents the average adhesion pressure measured over a period of 10 trials.

contact area, normal adhesion testing was performed with a flat PMMA probe. To ensure alignment of the flat probe to the magnetically controlled dry adhesive device, the flat PMMA with a surface area of 35.08 ± 0.01 mm^2 was gently placed on the surface of the device and then, using the linear stage, was bonded to a nylon screw attached directly to the load cell. After curing, normal adhesion tests were performed as described previously with no applied magnetic field and with the 0.0133 ± 0.0009 T magnetic field applied in either orientation 1 or orientation 2 during preloading. After applying an average preloading force of 1.510 ± 0.003 N, the normal adhesion pressure was measured to be 52.9 ± 0.5 kPa with no applied magnetic field present, 52.3 ± 0.7 kPa with the magnetic field applied in orientation 1, and 52.4 ± 0.4 kPa with the magnetic field applied in orientation 2. In other words, there was no significant difference in adhesion when the contact area remained constant regardless of the orientation of the magnetic field.

Interestingly, during the adhesion testing with the flat probe, it was found that the height of the magnetically controlled dry adhesive device changed depending on if the magnetic field was applied and the direction in which it was applied. The change in the height of the magnetically controlled dry adhesive device was determined by subtracting the linear stage position when the surface of the magnetically controlled dry adhesive device was first contacted from the linear stage position when the desired preload was achieved. With the magnetic field applied in orientation 1, the thickness of the magnetically controlled dry adhesive device increased by an average of 22.7 ± 0.9 μm but decreased by an average of 3.5 ± 1.0 μm with the magnetic field applied in orientation 2 on the basis of five tests each.

The increase or decrease in the overall thickness of the magnetically controlled dry adhesive device in the presence of a magnetic field is responsible for an increase or decrease in the contact area of the spherical probe. The increase or decrease in the contact area of the glass probe when the magnetic field is switched on is due to the linear stage (and thus the glass probe) being held stationary and the height of the magnetically controlled dry adhesive device increasing or decreasing. The increased thickness of the magnetically controlled dry adhesive when the magnetic field is in orientation 1 and when the glass probe is stationary potentially increases the contact radius from 553 to 610 μm. Similarly, with the magnetic field applied in orientation 2 when the glass probe is stationary, the overall height of the magnetically controlled dry adhesive device decreases, and consequently, the contact radius is potentially reduced from 553 to 543 μm. A diagram outlining the change in contact area is shown in Figure 8.

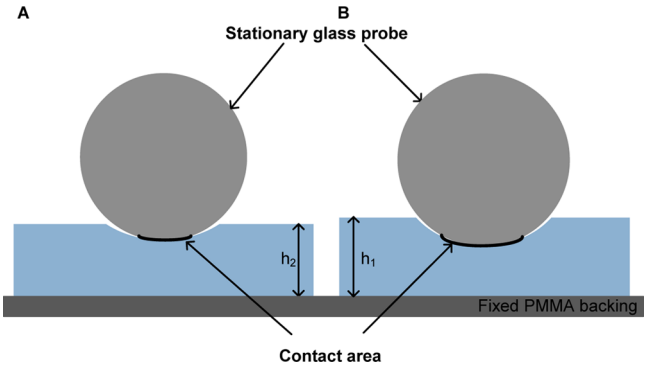

Figure 8. A diagram showing the increase in contact area because of the change in height of the device when the magnetic field is applied in orientation 1. (A) The sample is preloaded without the applied magnetic field present. (B) The magnetic field is switched on in orientation 1 and the height of the device increases resulting in increased contact area because the base of the device is fixed in place, and the glass probe remains stationary.

Figure 9 compares three typical force versus time curves which show the entire preload-pulloff normal adhesion test

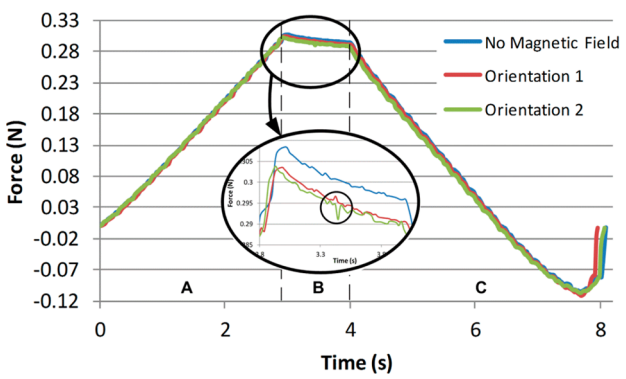

Figure 9. Typical force vs time curves during the entire preload-pulloff normal adhesion test cycle for when there was no applied magnetic field and when a 0.0133 ± 0.0009 T magnetic field was applied in either orientation 1 or orientation 2 during the pulloff portion of the test. Region A shows the increase in force as the magnetically controlled dry adhesive device is being preloaded. Region B shows a slight decrease in force as the sample relaxes while the glass probe is stationary while region C shows the decrease in force during the pulloff portion of the test. Negative forces indicate that the device is under tension. The inset shows a close-up view of the change in force with respect to time in region B, and the circled region within the inset shows the increase or decrease in force when the magnetic field is switched on resulting in increased or decreased contact area.

cycle when there is no applied magnetic field and when a 0.0133 ± 0.0009 T magnetic field is applied during the pulloff portion of the normal adhesion test cycle in both orientation 1 and orientation 2. Figure 9 breaks down the normal adhesion test cycle into three distinct regions: (A) the preload is being applied at a constant rate of 50 μm/s, (B) the linear stage and glass probe are held stationary and the magnetic field is switched on, and (C) the linear stage is moving in the reverse

DOI: 10.1021/am505140f
ACS Appl. Mater. Interfaces 2015, 7, 2214−2222

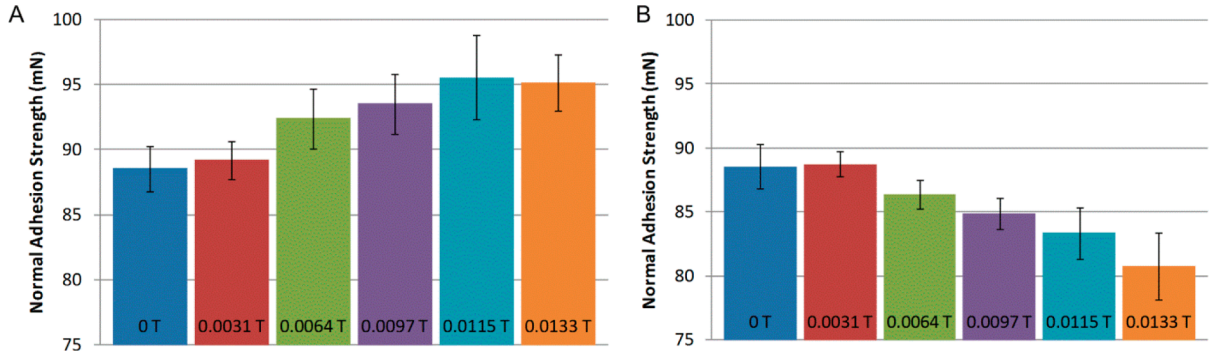

Figure 10. A comparison of the change in adhesion strength because of the presence of a magnetic field in (A) orientation 1 and (B) orientation 2. The magnetic field strength for each adhesion measurement is shown at the base of each column. Each data point represents the average of four trials, and the error bars indicate the standard deviation.

direction at a constant rate of 50 μm/s and the pulloff force is being measured. The circled region in the inset of Figure 9 shows that there is a small increasing spike in the measured preloading force when the magnetic field is switched on in orientation 1 and a small decreasing spike in the preloading force when the magnetic field is switched on in orientation 2 while the glass probe remains stationary. There is no sharp increase or decrease in the preloading force when there is no applied magnetic field. While the glass probe is stationary, the preloading force decreases as the material of the magnetically controlled dry adhesive device relaxes under the applied preload, and the rate of decrease of the measured preloading force, except for the increases or decreases in preload because of switching on the magnetic field, is at the same rate for all three cases.

To compare the effect of the magnetic field at varying strengths in both orientations 1 and 2, a series of tests were performed with a minimum of four trials per test. During each set of trials, normal adhesion force measurements were performed with the magnetic field applied in either orientation 1 or orientation 2 during the pulloff force measurements. The strength of the magnetic field was varied by decreasing the current through the coil, and normal adhesion force measurements were performed with magnetic field strengths of 0, 0.0031, 0.0064, 0.0097, 0.0115, and 0.0133 T. As can be seen in Figure 10 A and as summarized in Table 1, increasing the magnetic field strength with the magnetic field applied in orientation 1 during pulloff force measurements results in an increase in the normal adhesion force as compared to when no applied magnetic field is present. In Figure 10 B, a decrease in normal adhesion strength is seen as the magnetic field strength is increased, and the magnetic field is applied during pulloff force measurements in orientation 2. In both cases, an applied magnetic field strength of 0.0031 T or less appears to have a minimal effect on the measured normal adhesion force.

Table 1. Summary of the Normal Adhesion Test Results Shown in Figure 9 A and B

	magnetic field orientation 1		magnetic field orientation 2	
magnetic field strength (T)	preload force (mN)	pulloff force (mN)	preload force (mN)	pulloff force (mN)
0	299.6 ± 0.3	88.6 ± 1.8	299.6 ± 0.3	88.6 ± 1.8
0.0031	305.0 ± 1.3	89.2 ± 1.5	301.8 ± 0.5	88.8 ± 1.1
0.0064	307.6 ± 3.8	92.4 ± 4.4	301.9 ± 0.4	86.4 ± 1.2
0.0097	309.8 ± 5.7	93.6 ± 2.3	301.6 ± 0.6	84.9 ± 1.2
0.0115	313.4 ± 7.4	95.6 ± 3.2	302.6 ± 1.0	83.4 ± 2.0
0.0133	314.7 ± 6.6	95.1 ± 2.2	304.4 ± 2.0	80.8 ± 2.7

Finally, to determine if the adhesion test results previously shown for the protoype magnetically controlled dry adhesive device were repeatable with another device, a second magnetically controlled dry adhesive device was fabricated, and normal adhesion tests were performed with the 0.0133 ± 0.0009 T magnetic field present during only the pulloff portion of the adhesion test cycle. Figure 11 compares the % change in adhesion for the first sample (sample 1) and the second sample (sample 2) with the magnetic field applied in either orientation 1 or 2 over a series of five trials for each test. The % change in adhesion is compared to the normal adhesion force measurements performed without the applied magnetic present. The overall behavior of the two samples was similar even though the orientation of the magnetic field that resulted in the greatest % increase in adhesion force was different for each sample. The change in adhesion when in the presence of an applied magnetic field appears to be a function of the net magnetic field of the magnetically controlled dry adhesive device which is a function of the fabrication process. The direction of the net magnetic field of the magnetically controlled dry adhesive device is due to the fabrication process where mixing iron oxide particles into PDMS results in randomly aligned iron oxide

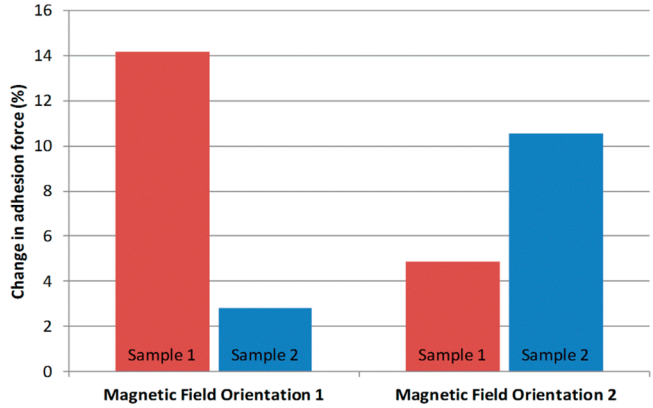

Figure 11. A comparison of the % change in adhesion between two magnetically controlled dry adhesive device samples when the samples were in the presence of a magnetic field and when no magnetic field was present. The adhesion data shown previously corresponds to sample 1. Each data point represents the average change in adhesion over five trials.

DOI: 10.1021/am505140f
ACS Appl. Mater. Interfaces 2015, 7, 2214−2222

particles within the uncured Fe-PDMS. Prior to curing, the particles are free to rotate within the uncured PDMS and can align themselves with each other or with an external magnetic field. In the future, a method of fabricating magnetically controlled adhesive devices which optimally improves overall adhesion should be developed and will likely involve curing the Fe-PDMS in the presence of a controlled magnetic field, which could result in a stronger net magnetic field over that which is presently observed along a greater change in adhesion in the presence of an applied magnetic field.

4. CONCLUSION

A method of fabricating magnetically controlled dry adhesive devices was developed. Using a coil, a magnetic field of up to 0.0133 ± 0.0009 T was generated and, when normal adhesion pressure measurements were performed, decreased normal adhesion pressures were measured when the applied magnetic field was present during the entire normal dry adhesive test cycle as compared to when there was no applied magnetic field present. Similarly, a decrease in adhesion was measured when the magnetic field was present during only the preload portion of the normal adhesion test cycle. In both cases, the decrease in adhesion pressure was due to an increase in the overall stiffness of the magnetically controlled dry adhesive device resulting in a smaller contact area with the spherical glass probe under the same preloading force. When the magnetic field was present during only the pulloff portion of the dry adhesion test cycle, the measured pulloff pressure increased when the applied magnetic field was in orientation 1 and decreased when the applied magnetic field was in orientation 2. With the magnetic field applied in orientation 1 when the device was preloaded, a spike in preloading force, because of the height of the device changing, was seen and was responsible for increasing the contact area which resulted in increased adhesion. When the magnetic field in orientation 2 was switched with the device preloaded, a decreasing spike in preload force was observed because of the thickness of the device decreasing, and a slight decrease in adhesion pressure was measured as compared to when no applied magnetic field was present. Multiple devices showed similar adhesion characteristics.

AUTHOR INFORMATION

Corresponding Author

*E-mail: Carlo_Menon@sfu.ca.

Author Contributions

The manuscript was written through contributions of all authors. All authors have given approval to the final version of the manuscript.

Notes

The authors declare no competing financial interest.

ACKNOWLEDGMENTS

This work was financially supported by The Natural Sciences and Engineering Research Council of Canada (NSERC).

REFERENCES

(1) Autumn, K.; Sitti, M.; Liang, Y. A.; Peattie, A. M.; Hansen, W. R.; Sponberg, S.; Kenny, T. W.; Fearing, R.; Israelachvili, J. N.; Full, R. J. Evidence for van Der Waals Adhesion in Gecko Setae. *Proc. Natl. Acad. Sci. U.S.A.* **2002**, *99*, 12252−12256.

(2) Autumn, K.; Liang, Y. A.; Hsieh, S. T.; Zesch, W.; Chan, W. P.; Kenny, T. W.; Fearing, R.; Full, R. J. Adhesive Force of a Single Gecko Foot-Hair. *Nature* **2000**, *405*, 681−685.

(3) Sitti, M. High Aspect Ratio Polymer Micro/Nano-Structure Manufacturing Using Nanoembossing, Nanomolding and Directed Self-Assembly. *ASME 2003 International Mechanical Engineering Congress and Exposition: Design Engineering, Volumes 1 and 2*, Washington, DC, November 15−21, 2003; pp 293−297.

(4) Geim, A. K.; Dubonos, S. V.; Grigorieva, I. V.; Novoselov, K. S.; Zhukov, A. A.; Shapoval, S. Y. Microfabricated Adhesive Mimicking Gecko Foot-Hair. *Nat. Mater.* **2003**, *2*, 461−463.

(5) Davies, J.; Haq, S.; Hawke, T.; Sargent, J. A Practical Approach to the Development of a Synthetic Gecko Tape. *Int. J. Adhes. Adhes.* **2009**, *29*, 380−390.

(6) Sameoto, D.; Menon, C. Direct Molding of Dry Adhesives with Anisotropic Peel Strength Using an Offset Lift-off Photoresist Mold. *J. Micromech. Microeng.* **2009**, *19*, 115026.

(7) Krahn, J.; Liu, Y.; Sadeghi, A.; Menon, C. A Tailless Timing Belt Platform (TBCP-II) Utilizing Dry Adhesives with Mushroom Caps. *Smart Mater. Struct.* **2011**, *20*, 115021.

(8) Krahn, J.; Menon, C. Characterization of Dry Adhesives Fabricated Using a Novel Mass Production Manufacturing Technique. *Macromol. React. Eng.* **2013**, *7*, 632−637.

(9) Greiner, C.; del Campo, A.; Arzt, E. Adhesion of Bioinspired Micropatterned Surfaces: Effects of Pillar Radius, Aspect Ratio, and Preload. *Langmuir* **2007**, *23*, 3495−3502.

(10) Jeong, H. E.; Lee, J.-K.; Kwak, H. N.; Moon, S. H.; Suh, K. Y. Effect of Leaning Angle of Gecko-Inspired Slanted Polymer Nanohairs on Dry Adhesion. *Appl. Phys. Lett.* **2010**, *90*.

(11) Spolenak, R.; Gorb, S.; Gao, H.; Arzt, E. Effects of Contact Shape on the Scaling of Biological Attachments. *Proc. R. Soc. A* **2005**, *461*, 305−319.

(12) Varenberg, M.; Gorb, S. Close-up of Mushroom-Shaped Fibrillar Adhesive Microstructure: Contact Element Behaviour. *J. R. Soc. Interface* **2008**, *5*, 785−789.

(13) del Campo, A.; Greiner, C.; Arzt, E. Contact Shape Controls Adhesion of Bioinspired Fibrillar Surfaces. *Langmuir* **2007**, *23*, 10235−10243.

(14) Parsaiyan, H.; Barazandeh, F.; Mehdirezaei, S.; Parsaiyan, M.; Safdari, M. Wide-End Fibers and Their Adhesion Performance in Biological Attachment Systems. *Int. J. Adhes. Adhes.* **2009**, *29*, 444−450.

(15) Jeong, H. E.; Suh, K. Y. Nanohairs and Nanotubes: Efficient Structural Elements for Gecko-Inspired Artificial Dry Adhesives. *Nano Today* **2009**, *4*, 335−346.

(16) Kwak, M. K.; Pang, C.; Jeong, H.-E.; Kim, H.-N.; Yoon, H.; Jung, H.-S.; Suh, K.-Y. Towards the Next Level of Bioinspired Dry Adhesives: New Designs and Applications. *Adv. Funct. Mater.* **2011**, *21*, 3606−3616.

(17) Sameoto, D.; Menon, C. Recent Advances in the Fabrication and Adhesion Testing of Biomimetic Dry Adhesives. *Smart Mater. Struct.* **2010**, *19*, 103001.

(18) Krahn, J.; Sameoto, D.; Menon, C. Controllable Biomimetic Adhesion Using Embedded Phase Change Material. *Smart Mater. Struct.* **2011**, *20*, 015014.

(19) Kim, S.; Sitti, M.; Xie, T.; Xiao, X. Reversible Dry Micro-Fibrillar Adhesives with Thermally Controllable Adhesion. *Soft Matter* **2009**, *5*, 3689.

(20) Reddy, S.; Arzt, E.; del Campo, A. Bioinspired Surfaces with Switchable Adhesion. *Adv. Mater.* **2007**, *19*, 3833−3837.

(21) Arul, E. P.; Ghatak, A. Control of Adhesion via Internally Pressurized Subsurface Microchannels. *Langmuir* **2012**, *28*, 4339−4345.

(22) Nadermann, N.; Ning, J.; Jagota, A.; Hui, C.-Y. Active Switching of Adhesion in a Film-Terminated Fibrillar Structure. *Langmuir* **2010**, *26*, 15464−15471.

(23) Jeong, H. E.; Kwak, M. K.; Suh, K. Y. Stretchable, Adhesion-Tunable Dry Adhesive by Surface Wrinkling. *Langmuir* **2010**, *26*, 2223−2226.

(24) Krahn, J.; Menon, C. Electro-Dry-Adhesion. *Langmuir* **2012**, *28*, 5438−5443.

DOI: 10.1021/am505140f
ACS Appl. Mater. Interfaces 2015, 7, 2214−2222

(25) Krahn, J. M.; Pattantyus-Abraham, A. G.; Menon, C. Polymeric Electro-Dry-Adhesives for Use on Conducting Surfaces. *Proc. Inst. Mech. Eng., Part L* **2013**, *228*, 109−114.
(26) Ruffatto, D., III; Parness, A.; Spenko, M. Improving Controllable Adhesion on Both Rough and Smooth Surfaces with a Hybrid Electrostatic/gecko-like Adhesive. *J. R. Soc. Interface* **2014**, *11*, 20131089.
(27) Berengueres, J.; Takahashi, K. *Magnetic Hair for Wall Mobility*. *Proceedings of the 2006 IEEE/RSJ International Conference on Intelligent Robots and Systems*, Beijing, Oct 9−15, 2006.
(28) Gillies, A. G.; Kwak, J.; Fearing, R. S. Controllable Particle Adhesion with a Magnetically Actuated Synthetic Gecko Adhesive. *Adv. Funct. Mater.* **2013**, *23*, 3256−3261.
(29) Northern, M. T.; Greiner, C.; Arzt, E.; Turner, K. L. A Gecko-Inspired Reversible Adhesive. *Adv. Mater.* **2008**, *20*, 3905−3909.
(30) Tian, T. F.; Zhang, X.; Li, W.; Alici, G.; Ding, J. Study of PDMS Based Magnetorheological Elastomers. *J. Phys. (Paris)* **2013**, *412*, 1−8.
(31) Li, W.; Nakano, M. Fabrication and Characterization of PDMS Based Magnetorheological Elastomers. *Smart Mater. Struct.* **2013**, *22*, 055035/1−055035/7.
(32) Varga, Z.; Filipcsei, G.; Zrínyi, M. Magnetic Field Sensitive Functional Elastomers with Tuneable Elastic Modulus. *Polymer (Guildf).* **2006**, *47*, 227−233.
(33) Filipcsei, G.; Csetneki, I.; Szilágyi, A.; Zrínyi, M. Magnetic Field-Responsive Smart Polymer Composites. *Adv. Polym. Sci. Polym. Sci.* **2007**, *206*, 137−189.
(34) Li, J.; Zhang, M.; Wang, L.; Li, W.; Sheng, P.; Wen, W. Design and Fanbrication of a Microfluidic Mixer from Carbonyl Iron-PDMS Composite Membrane. *Microfluid. Nanofluid.* **2011**, *10*, 919−925.
(35) Varga, Z.; Filipcsei, G.; Szilágyi, A.; Zrínyi, M. Electric and Magnetic Field-Structured Smart Composites. *Macromol. Symp.* **2005**, *227*, 123−134.
(36) Varga, Z.; Filipcsei, G.; Zrínyi, M. Smart Composites with Controlled Anisotropy. *Polymer (Guildf).* **2005**, *46*, 7779−7787.
(37) Long, R.; Hui, C.-Y.; Kim, S.; Sitti, M. Modeling the Soft Backing Layer Thickness Effect on Adhesion of Elastic Microfiber Arrays. *J. Appl. Phys.* **2008**, *104*, 044301.
(38) Kim, S.; Sitti, M.; Hui, C.-Y.; Long, R.; Jagota, A. Effect of Backing Layer Thickness on Adhesion of Single-Level Elastomer Fiber Arrays. *Appl. Phys. Lett.* **2007**, *91*, 161905.
(39) Krahn, J.; Menon, C. Dry Adhesives with Sensing Features. *Smart Mater. Struct.* **2013**, *22*, 085010.
(40) del Campo, A.; Greiner, C.; Arzt, E. Contact Shape Controls Adhesion of Bioinspired Fibrillar Surfaces. *Langmuir* **2007**, *23*, 10235−10243.

DOI: 10.1021/am505140f
ACS Appl. Mater. Interfaces 2015, 7, 2214−2222